ADVANCED MATERIALS

Supporting Information

for *Adv. Mater.,* DOI: 10.1002/adma.202106633

Super-Resolution Imaging of Highly Curved Membrane Structures in Giant Vesicles Encapsulating Molecular Condensates

Ziliang Zhao, Debjit Roy, Jan Steinkühler, Tom Robinson, Reinhard Lipowsky, and Rumiana Dimova**

Supporting Information

Super-resolution imaging of highly curved membrane structures in giant vesicles encapsulating molecular condensates

Ziliang Zhao[1,2,3]*, *Debjit Roy*[1,4], *Jan Steinkühler*[1,5], *Tom Robinson*[1], *Reinhard Lipowsky*[1] *and Rumiana Dimova*[1]*

[1]Department of Theory and Bio-Systems, Max Planck Institute of Colloids and Interfaces, Science Park Golm, 14424 Potsdam, Germany
[2]Department of Biophysical Imaging, Leibniz Institute of Photonic Technology, 07745 Jena, Germany
[3]Faculty of Physics and Astronomy, Institute of Applied Optics and Biophysics, Friedrich Schiller University Jena, 07743 Jena, Germany
[4]Present address: Department of Biochemistry and Molecular Biophysics, Washington University School of Medicine, St. Louis, Missouri, 63110, USA
[5]Present address: Department of Biomedical Engineering, Northwestern University, Evanston, IL 60657, USA
* Address correspondence to Ziliang.Zhao@leibniz-ipht.de, Rumiana.Dimova@mpikg.mpg.de

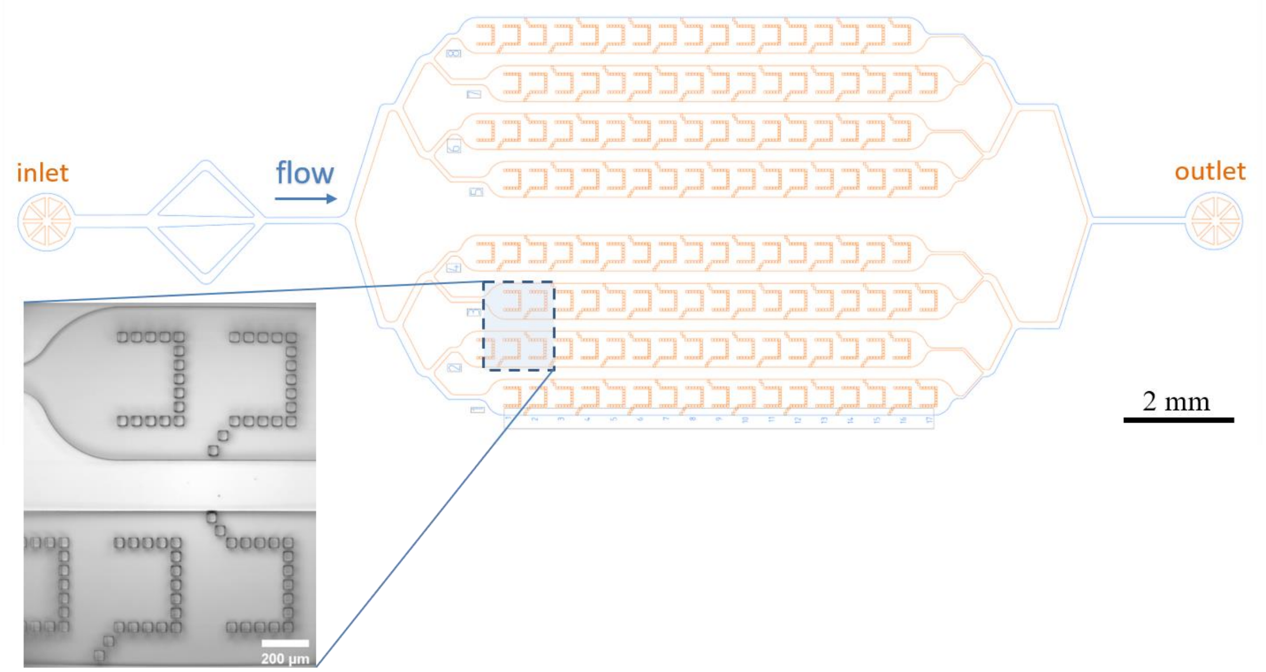

Figure S1. Sketch of the microfluidic chip used for trapping GUVs with an 8-channel cascade GUV trapping system (12-channel systems were also used). The flow channel splits into 8 separate lines, each with 17 traps with a total of 136 traps per device. The image on the left shows a magnified bright-field image of the chip with several traps.

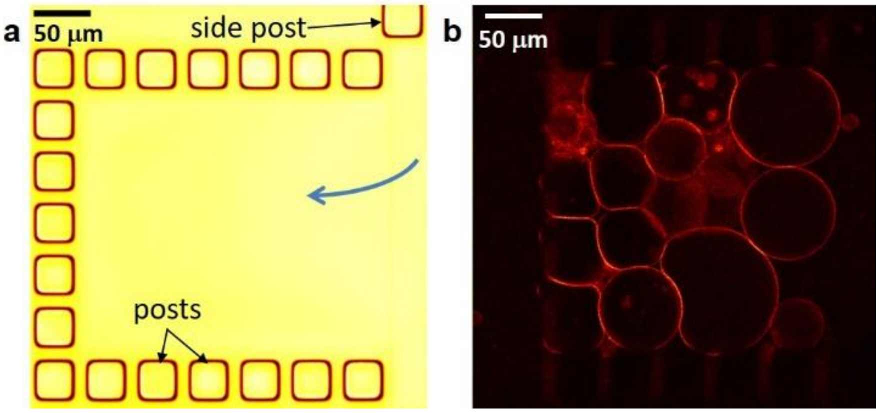

Figure S2. Microfluidic trapping of GUVs. (a) Posts of a single microfluidic trap viewed in transmission mode. The blue arrow shows the direction of the incoming GUVs. The PDMS posts have the lateral dimensions of 35 µm × 35 µm and a height of 70 µm. (b) Confocal image of GUVs trapped by the posts in the microfluidic device. Some GUVs are slightly deformed by the applied flow (1.0 µL/min).

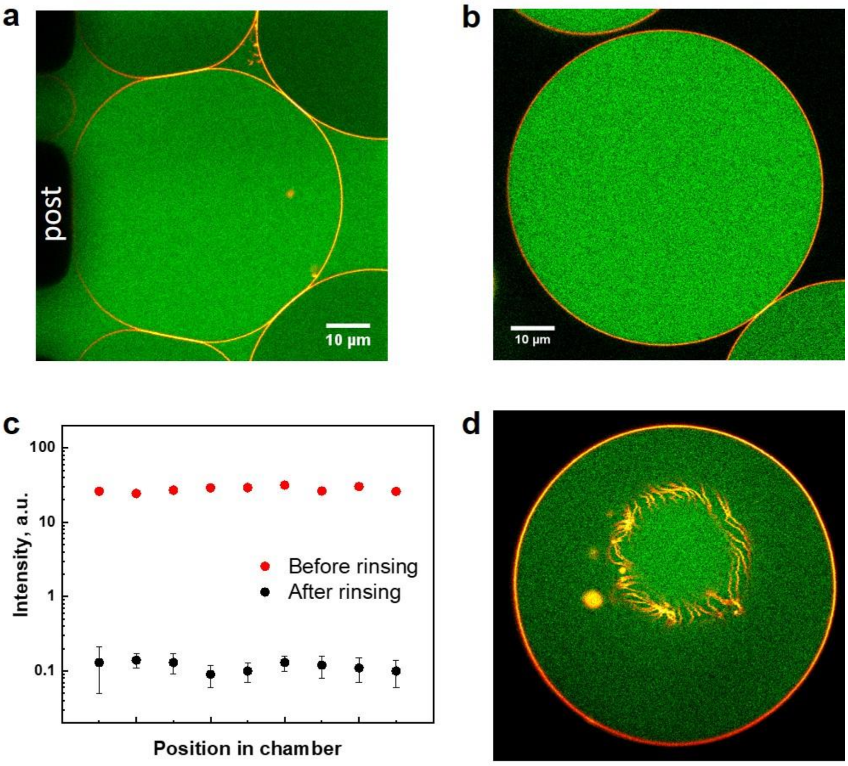

Figure S3. Solution exchange efficiency in the microfluidic device and ATPS encapsulation in the GUVs. (a) GUVs in the electroformation medium (containing FITC-dextran, green) are trapped by the posts of the microfluidic chip. (b) Confocal xy scan of GUVs after the 1st deflation step: the external fluorescence signal is close to zero, meaning the solution exchange outside the GUVs is complete. The GUVs remaining in the chip after the 1st deflation step have similar fluorescence intensities (this indicates that vesicles not encapsulating the correct amount of polymers were lost during this washing step). (c) The fluorescence signal at random positions in the device (inlet, outlet, in between GUVs, next to the trapping posts etc.) was measured before and after rinsing; intensity of ~0.1 a.u. (note the logarithmic scale) denotes that the solution exchange efficiency is ~100%. 3 to 4 measurements per position in the chamber were done from 3 preparation repeats; the error bar show standard deviations. (d) Confocal xy scan of one GUV after the 2nd deflation step (with deflation ratio r = 1.4 as defined by the ratio of external osmolarity to the initial osmolarity of the solution inside the vesicle) resulting in phase separation in the GUV and accumulation of tubes at the two-phase interface; the fluorescence intensity of the dextran-rich phase (seen in the middle) is higher than that of the PEG-rich phase (in the rest of the GUV interior).

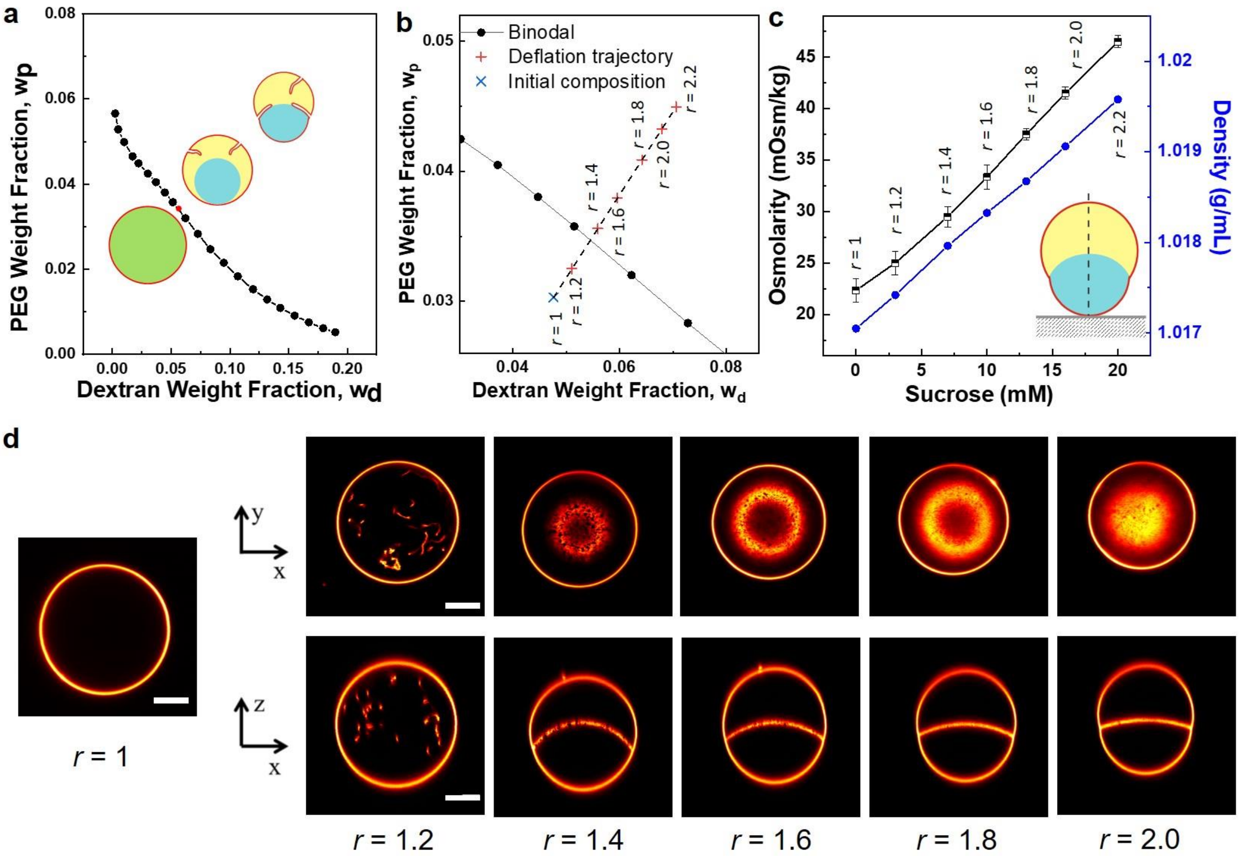

Figure S4. Phase diagram of PEG-dextran solutions and conditions at the individual deflation steps. (a) High-precision phase diagram of PEG and dextran aqueous solutions at 23.5 ± 1°C. The red dot indicates the location of the critical point. Below the binodal, the polymer solution is homogeneous; above the binodal it undergoes phase separation into two aqueous phases. The insets illustrate the morphology change of a vesicle along the deflation trajectory. (b) Deflation trajectory shown at higher resolution (the graph represents a zoomed-in portion of panel a). (c) Osmolarity and density of the external deflation medium altered by the addition of sucrose; the respective deflation ratio *r* is indicated. The osmolarity of the external solution (black data, left axis) is increased in a step-wise manner with each step about 20% of the original value. The density of the external solution (blue data, right axis) is kept between the densities of the PEG-rich (yellow) and the dextran-rich (blue) phases in the vesicle so that the deflated vesicle stands vertically on the coverslip as sketched in the inset. The data points indicate the initial isotonic condition with a lower density as well as the six successive deflation steps. (d) Osmotic deflation and spontaneous tubulation of one GUV at different deflation steps along the deflation trajectory with increasing osmolarity of the external solution. After the 2nd and onwards deflation steps, the internal solution in the vesicle undergoes phase separation and the nanotubes adhere at the interface. At higher deflation levels, the overcrowded nanotubes appear to be blurry due to the poor confocal lateral resolution. Scale bars:10 µm.

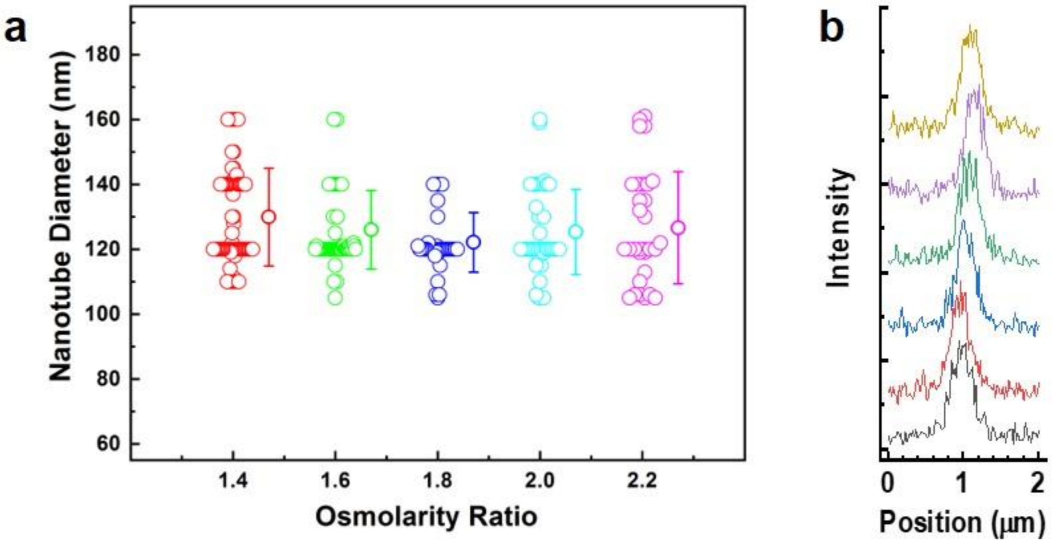

Figure S5. (a) Manual analysis of intensity line scans obtained with 3D STED of vesicles exposed to different osmotic deflation conditions as defined by the osmolarity ratio *r*, between the external solution and the initial osmolarity of the solution in the vesicle. As the nanotubes were constantly moving, a pixel size of 15/20 nm was chosen. The individual data points in the graph represent measurements on different tubes. Average and standard deviation are indicated on the right. For *r* = 1.4, a total of 76 line scans of 45 nanotubes were analyzed. For *r* = 1.6, a total of 77 line scans of 54 nanotubes were analyzed; for *r* = 1.8, 41 line scans on 33 nanotubes; for *r* = 2.0, 47 line scans on 33 nanotubes; for *r* = 2.2, 34 line scans on 17 nanotubes. In total, 15200 line scans have been collected. On average, 98.2% of the line scans were discarded as they did not show two clear peaks (as illustrated in panel b). The average value for the nanotube diameter for all deflation levels is ~125 nm. High deflation was not attempted due to the crowding of nanotubes at the two-phase interface. (b) A series of six 3D STED line scans on the same nanotube. Due to movement, the line scans do not always exhibit two major peaks reflecting the tube wall crossing. In this set of measurements, only the blue line (3^{rd} line from the bottom) shows only two major peaks of comparable height and is considered for manual analysis. Due to lateral movement, the peak maxima deviate also in x-position. The time between the first and last 3D STED line scans is 40 milliseconds.

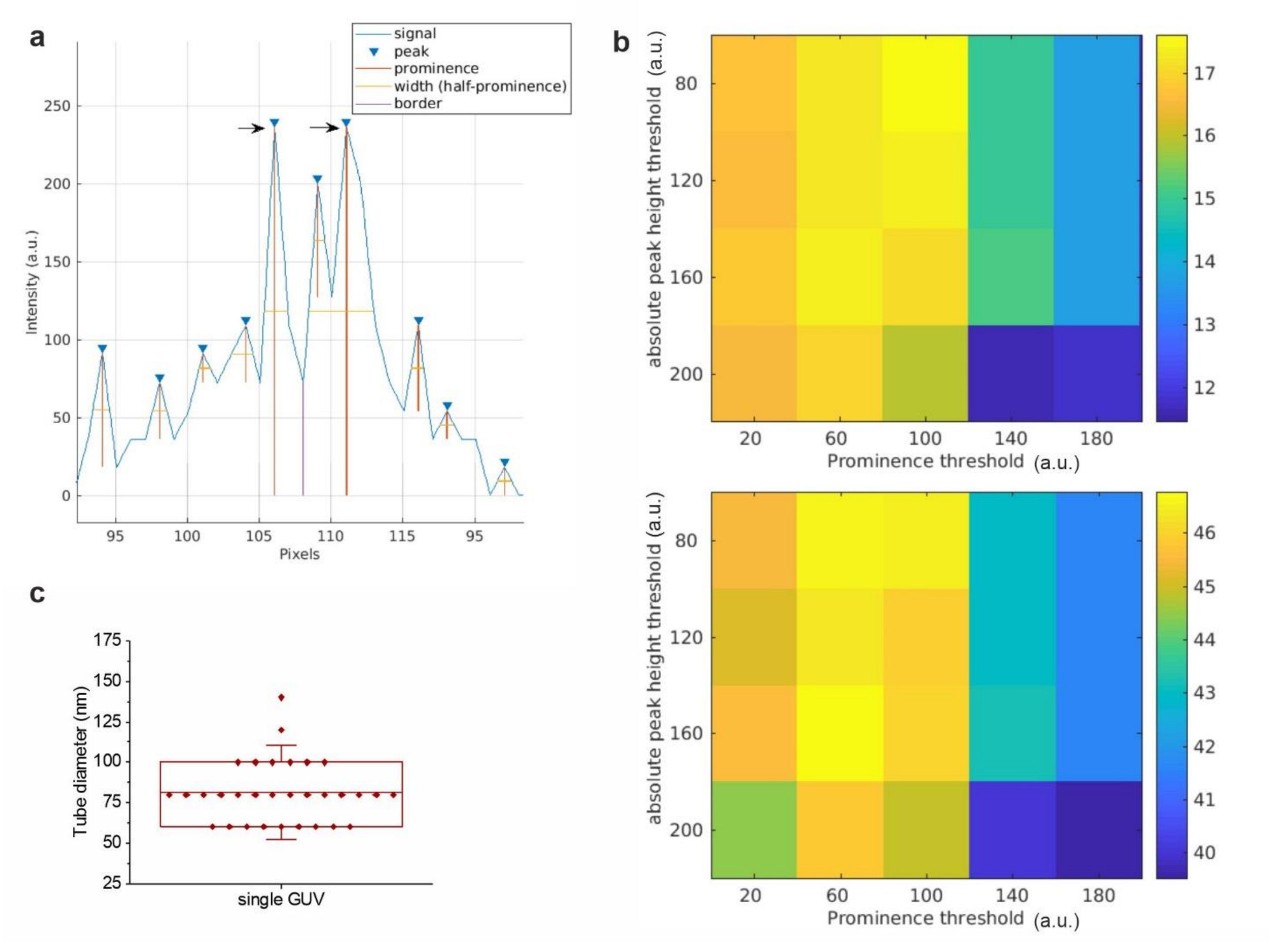

Figure S6. Automated analysis of 3D STED line scans across membrane nanotubes illustrated for tubes at deflation ratio $r = 1.4$. (a) Example line scan across a nanotube given for illustration purposes. The pixel size is 20 nm. The calculated quantity of the peak prominence is shown by the length of the vertical red lines. The black arrows point to the two most prominent peaks chosen for the nanotube diameter calculation for the typical parameter set of thresholds. (b) Color-coded maps of the standard deviation (top) and mean nanotube radius (bottom) in units of nm of a single GUV used to calibrate the threshold parameters of peak and prominence thresholds. (c) Distribution of the nanotube diameters of a single GUV obtained by the optimal parameter corresponding to lowest standard deviation (peak and prominence thresholds 200 and 140 a.u., respectively, which correspond to the lowest standard deviation, as shown by the darkest blue pixel). Each data point corresponds to a different line scan (32 in total) on a single nanotube.

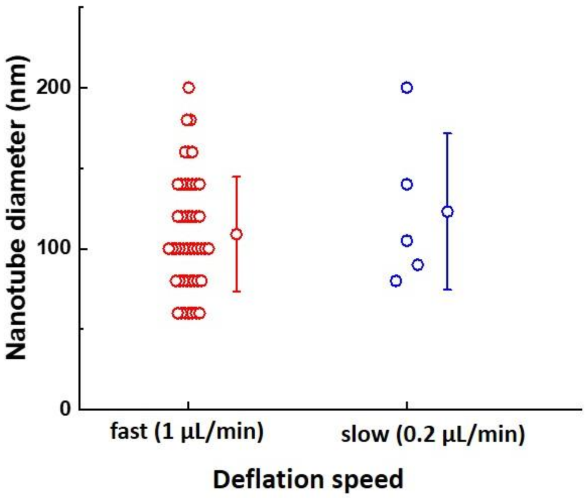

Figure S7. Nanotube diameter comparison between normal deflation and low deflation speed (*r* = 1.4), both analyzed by the automated image analysis method. Nanotube diameter for deflation speed of 1 µl/min is 109 nm (S.D. of 35 nm), and for deflation speed of 0.2 µl/min is 123 nm (S.D. of 49 nm). Acquiring the data at slow deflation takes very long (>200 min), which results in the poorer statistics.

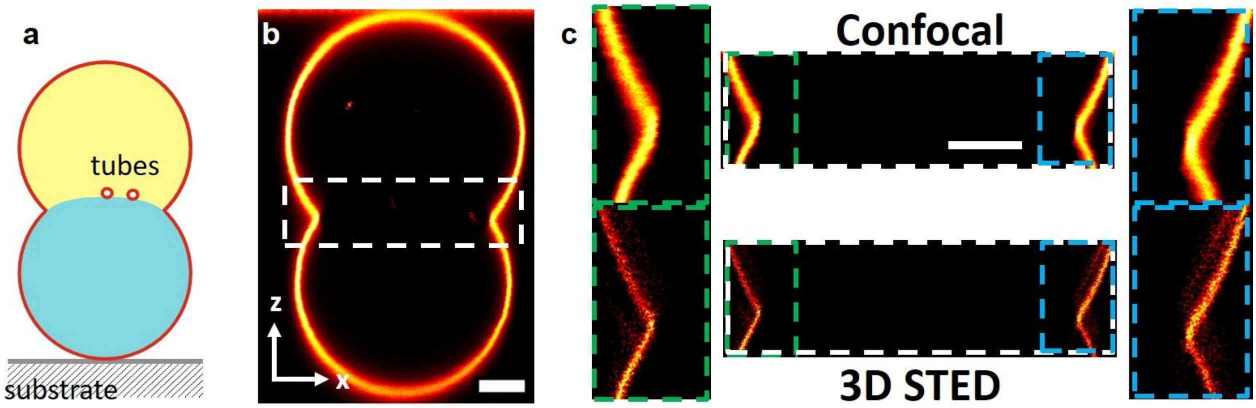

Figure S8. Imaging GUVs standing upright (in bulk) and the “kink” region. (a) Sketch of a budded vesicle with phase-separated interior. (b) Confocal xz scan of a budded GUV at a pixel size of 100 nm. The membrane neck region appears as a “kink” due to the poor axial resolution. (c) Zoomed-in segments acquired with confocal (top) and 3D STED with pixel size of 55 nm (bottom). The middle image corresponds to the rectangular region shown with white dashed line in (b). The left and right panels correspond to enlarged segments of the middle panel showing the left and right sides of the membrane neck as indicated by the colored rectangular regions. Due to the poor axial resolution in confocal mode (~446 nm), the membrane neck cannot be resolved and appears as a straight line, the corresponding 3D STED resolved the membrane neck in more details due to its better axial resolution of ~120 nm, but as the resolution is on the same order of magnitude with the membrane curvature, a sharper detail on the neck could not be achieved as compared with Fig. 7c in the main text. Scale bars: 5 µm.

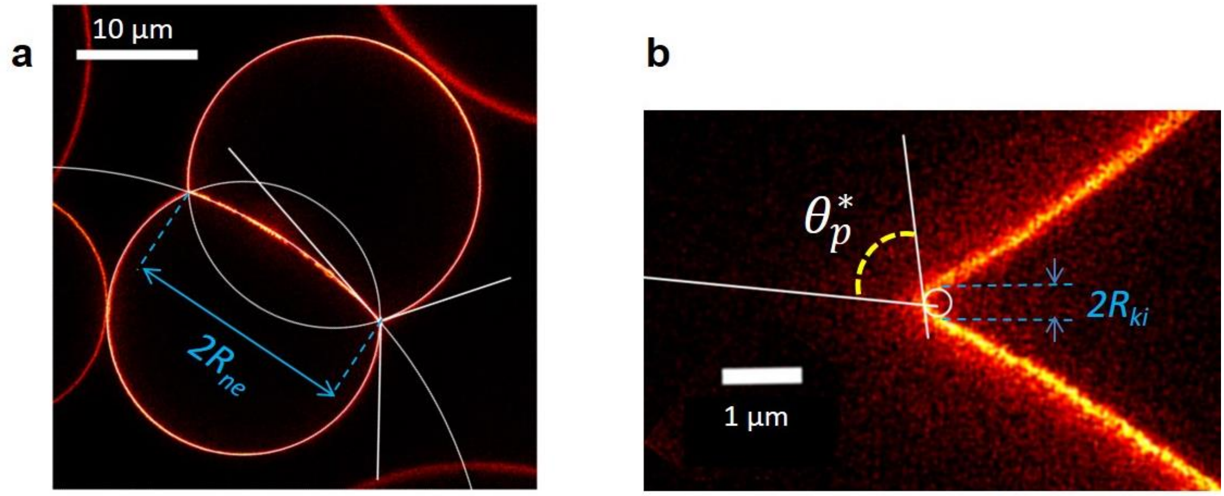

Figure S9. Measuring the apparent and intrinsic contact angles from confocal and STED images. (a) The spherical cap segments of the vesicle and interface contours are fitted to circles (white curves). The tangent lines are drawn based on the center of the circle and the contact point at the circle from which the apparent contact angles θ_p, θ_d and θ_e can be determined, see sketch in Fig. 7a for angle definition. The fluorescent intensity of nanotubes at the interface makes it impossible to image the “kink” region with clear details in such vesicles. The neck radius, R_{ne}, used to assess the mean curvature in the “kink” region is also indicated. (b) A clean interface near the “kink” region facilitates clear readout of “kink” fluorescent signal. To measure the intrinsic contact angle θ_p^* from STED images, the curved membrane contour in the “kink” region is fitted to a circle with radius R_{ki}. The contour of the two-phase interface is obtained from the full-vesicle image (as shown in Fig. 7b). The tangents (white lines) form the intrinsic contact angle θ_p^*.

Supporting Movies

Movie S1: Nanotube fluctuation at the ATPS interface. The movie captures the fluctuation of two nanotubes at the interface after the 2nd deflation step (r = 1.4) using confocal microscopy. The nanotubes are constantly moving along the two-phase interface. The imaging area is 4×2 µm, pixel size was set to 100 nm to allow fast video capture.

Movie S2: Nanotube movement used to illustrate the tube persistence length. Nanotubes in a vesicle at r = 1.6 are undulating with persistence length around 5.9 µm (S.D. of 3.9 µm) as captured with STED, suggesting cylindrical structure of the tubes. With time, some of the nanotubes leave the imaging area resulting from the optical tweezer effect of the STED laser.

Movie S3: Membrane neck of an ATPS budding GUV. The thermal undulation of the membrane neck was captured with 2D STED. The real curvature of the membrane neck can be revealed (with higher intensities on the membrane showing the two buds are in sharp focus) but with time the equators of the two buds are getting out of focus due to membrane undulations; this adds some uncertainty when analyzing the membrane neck radius.